AAAS
Research
Volume 2019, Article ID 6439734, 10 pages
https://doi.org/10.34133/2019/6439734

Research
A SCIENCE PARTNER JOURNAL

Research Article

A General Method for the Synthesis of Hybrid Nanostructures Using $MoSe_2$ Nanosheet-Assembled Nanospheres as Templates

Shikui Han,[1,2] **Kai Zhou**,[2,3,4] **Yifu Yu**,[2] **Chaoliang Tan**,[2] **Junze Chen**,[2] **Ying Huang**,[2] **Qinglang Ma**,[2] **Ye Chen**,[2] **Hongfei Cheng**,[2] **Weijia Zhou**,[4] **and Hua Zhang**[2,5]

[1]*Key Laboratory of Advanced Catalytic Materials and Reaction Engineering, School of Chemistry and Chemical Engineering, Hefei University of Technology, Hefei 230009, China*
[2]*Center for Programmable Materials, School of Materials Science and Engineering, Nanyang Technological University, 50 Nanyang Avenue, Singapore 639798*
[3]*Center for Advanced Analytical Science, School of Chemistry and Chemical Engineering, Guangzhou University, Guangzhou 510006, China*
[4]*New Energy Research Institute, School of Environment and Energy, South China University of Technology, Guangzhou Higher Education Mega Center, Guangzhou 510006, China*
[5]*Department of Chemistry, City University of Hong Kong, Tat Chee Avenue, Kowloon, Hong Kong*

Correspondence should be addressed to Hua Zhang; hua.zhang@cityu.edu.hk

Received 26 April 2019; Accepted 16 September 2019; Published 14 November 2019

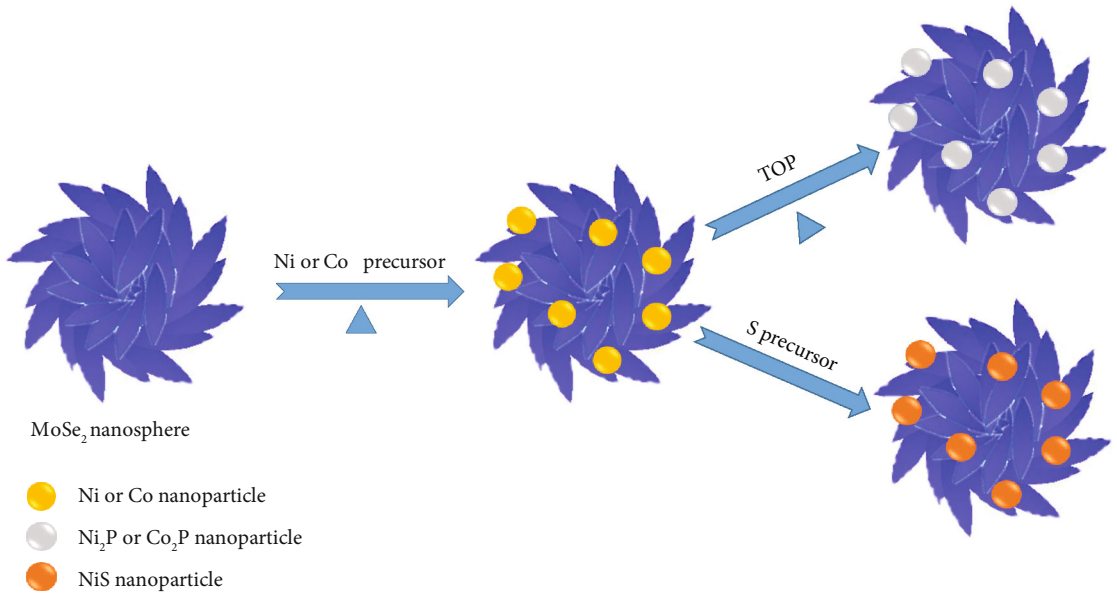
Copyright © 2019 Shikui Han et al. Exclusive Licensee Science and Technology Review Publishing House. Distributed under a Creative Commons Attribution License (CC BY 4.0).

The layered transition metal dichalcogenides (TMDs) and transition metal phosphides are low-cost, earth-abundant, and robust electrocatalysts for hydrogen evolution reaction (HER). Integrating them into hybrid nanostructures is potentially promising to further boost the catalytic activity toward HER based on their synergistic effects. Herein, we report a general method for the synthesis of a series of $MoSe_2$-based hybrid nanostructures, including $MoSe_2$-Ni_2P, $MoSe_2$-Co_2P, $MoSe_2$-Ni, $MoSe_2$-Co, and $MoSe_2$-NiS, by postgrowth of Ni_2P, Co_2P, Ni, Co, and NiS nanostructures on the presynthesized $MoSe_2$ nanosheet-assembled nanospheres, respectively, via a colloidal synthesis method. As a proof-of-concept application, the as-synthesized hybrid nanostructures are used as electrocatalysts for HER, exhibiting high activity and stability in acidic media. Among them, the $MoSe_2$-Co_2P composite shows the highest HER activity with an overpotential of 167 mV at 10 mA cm^{-2}.

1. Introduction

With increasing concerns on the global environmental contamination and energy shortage caused by the excessive consumption of fossil fuels, hydrogen as a promising chemical fuel has been considered as a clean and sustainable alternative [1–4]. However, the massive and sustainable hydrogen production from the electrocatalytic water splitting requires highly efficient and robust catalysts [5–9]. Although platinum (Pt) and other precious metals have shown superior catalytic performance in the hydrogen evolution reaction (HER) at low overpotentials in acidic media, their scarcity and high cost limit their practical applications [10–12]. Therefore, it is still a great challenge to find cost-effective and earth-abundant electrocatalysts with high HER activity, low overpotential, and excellent stability to replace the rare and expensive noble metal electrocatalysts.

Among various non-noble-metal HER catalysts, transition metal semiconductor nanomaterials, e.g., dichalcogenides and phosphides, have been extensively studied [13–21], because of their low cost, high abundancy, and high HER catalytic activity [22–28]. Recently, theoretical calculations and experimental studies on MoS_2 nanosheets suggested that the exposed edge is one of the catalytically active sites for hydrogen evolution [29, 30], which inspired researchers to prepare edge-rich MoS_2 nanostructures to enhance the HER performance [31–34]. Furthermore, based on the density functional theory, Tsai et al. found that the HER performance



Scheme 1: Schematic illustration of synthesis of the $MoSe_2$ nanosphere-based hybrid nanostructures.

of $MoSe_2$ can be comparable to or even better than that of MoS_2 [35]. However, there are only a few reports on designing the catalytically active $MoSe_2$ nanostructures for HER [36–41]. Besides transition metal dichalcogenides (TMDs), the emerging transition metal phosphides have also drawn extensive attention as effective HER catalysts due to their good durability, corrosion resistance, and high current density at low overpotential [42–50]. Among them, the Co- and Ni-based phosphide nanostructures have exhibited their great potential as the electrocatalysts for HER [26, 51–54]. Therefore, it is very important to design and synthesize $MoSe_2$-based hybrid HER electrocatalysts by combining the advantages of both $MoSe_2$ and transition metal phosphides. Herein, we report a general colloidal method for the synthesis of a series of hybrid nanostructures using the $MoSe_2$ nanosheet-assembled nanospheres as templates, including $MoSe_2$-Ni_2P, $MoSe_2$-Co_2P, $MoSe_2$-Ni, $MoSe_2$-Co, and $MoSe_2$-NiS (Scheme 1). First, $MoSe_2$ nanospheres were prepared by a hot-injection method. Then, the obtained $MoSe_2$ nanospheres mixed with transition metal cations, oleylamine, and trioctylphosphine in a three-necked flask. Because the surface potential of the freshly prepared $MoSe_2$ nanospheres is negative, the transition metal cations in the solution can be easily adsorbed on the surface of $MoSe_2$ nanosheets via the electrostatic interaction. As shown in Scheme 1, when the reaction temperature was increased to about 220°C, Ni or Co nanoparticles were formed. If the reaction temperature was further increased to 320°C, the trioctylphosphine would react with transition metals to form the transition metal phosphides on $MoSe_2$ nanospheres. However, if the reaction temperature was 220°C, after addition of the S precursor, the transition metal sulfide, such as NiS, nanoparticles were formed on $MoSe_2$ nanospheres. As a proof-of-concept application, the as-prepared hybrid nanostructures exhibit high electrocatalytic HER activity and stability in acidic media.

2. Results

Briefly, the colloidal $MoSe_2$ nanosheet-assembled nanospheres were prepared by injection of the selenium-octadecene precursor into a mixture of octadecene and stearic acid containing $MoCl_5$ at 300°C, which was kept for 30 min (see Materials and Methods for details). The morphologies of the obtained colloidal $MoSe_2$ nanospheres were characterized by a transmission electron microscope (TEM). As shown in Figures 1(a) and 1(b), the prepared $MoSe_2$ nanospheres with size of 75 ± 7 nm (inset in Figure 1(b)) were formed by the assembly of $MoSe_2$ nanosheets. High-resolution TEM (HRTEM) image of a typical edge of $MoSe_2$ nanosheet confirms its single-crystalline nature (Figure 1(c)). The lattice distances of 2.88 Å and 6.89 Å can be assigned to the (100) and (002) planes of 2H phase $MoSe_2$ [37], respectively (Figures 1(c) and 1(d)). The powder X-ray diffraction (XRD) pattern (Figure S1) further confirms that the nanosphere consists of crystalline 2H phase $MoSe_2$ (JCPDS No. 15-0029, hexagonal, $a = 3.288$ Å, $c = 12.89$ Å). As shown in Figure S1, the peaks located at 31.69°, 37.38°, and 56.10° correspond to the (100), (103), and (110) planes of the hexagonal $MoSe_2$, respectively.

The as-prepared $MoSe_2$ nanosheet-assembled nanospheres were then used as templates for the growth of hybrid nanostructures. For example, Ni_2P nanoparticles have been grown on the surface of $MoSe_2$ nanospheres to form the $MoSe_2$-Ni_2P hybrid nanostructures (see Materials and Methods for details). From the TEM image (Figure 2(a)), it can be seen that the Ni_2P nanoparticles are coated on the surface of $MoSe_2$ nanospheres. Based on the XRD analysis (Figure S2), the as-obtained hybrid nanostructure is composed of crystalline 2H phase of $MoSe_2$ (JCPDS No. 15-0029) and hexagonal phase of Ni_2P (JCPDS No. 65-1989, $a = 5.859$ Å, $c = 3.382$ Å). The HRTEM image (Figure 2(b)) further confirms that the Ni_2P nanoparticles are highly crystalline with a lattice spacing of 2.31 Å attributing to the

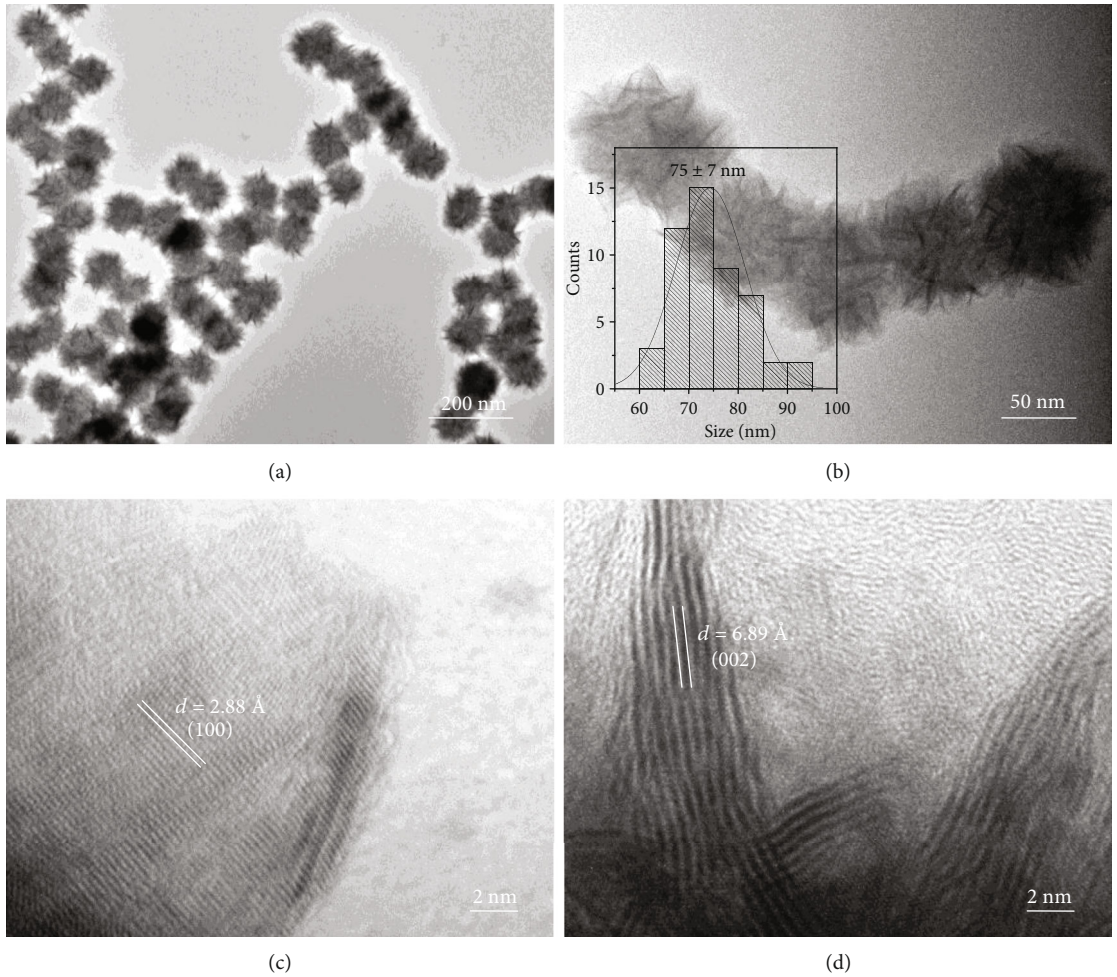


Figure 1: TEM and HRTEM measurements of the as-prepared $MoSe_2$ nanospheres. (a, b) TEM images and (c, d) HRTEM images. Inset in (b): statistical analysis of the size of 50 $MoSe_2$ nanospheres measured from TEM images.

(111) planes of the hexagonal phase Ni_2P. The measured lattice distance of 6.89 Å corresponds to the (002) plane of 2H phase $MoSe_2$. The size of Ni_2P nanoparticles in the hybrid nanostructures is 8.7 ± 1.3 nm (Figure S3). The energy-dispersive X-ray spectroscopy (EDS) spectrum (Figure S4) shows that the estimated molar ratios of Mo/Se and Ni/P are 1/2.2 and 1.6/1, respectively, close to the calculated stoichiometric ratios. The corresponding EDS elemental mapping (Figure S5) confirms the homogeneous distribution of Mo, Se, Ni, and P, further revealing the successful growth of Ni_2P on the surface of $MoSe_2$ nanospheres.

Importantly, our method is general, which can be used to grow other nanostructures on $MoSe_2$ nanospheres. For example, Co_2P nanoparticles can also be grown on the surface of $MoSe_2$ nanospheres to form $MoSe_2$-Co_2P hybrid nanostructures (Figure 2(c)). The measured lattice fringes of 6.89 Å and 2.23 Å match well with the (002) planes of $MoSe_2$ and (121) planes of Co_2P, respectively. The size of Co_2P nanoparticles in the hybrid nanostructures is 7.5 ± 1.4 nm (Figure S6). The XRD analysis (Figure S7) demonstrates the coexistence of $MoSe_2$ (JCPDS No. 15-0029) and Co_2P (JCPDS No. 32-0306, orthorhombic, $a = 5.6465\,Å$, $b = 6.6099\,Å$, $c = 3.513\,Å$). The molar ratios of Mo/Se and Co/P are 1/1.5 and 2.2/1, respectively, as characterized by EDS (Figure S8). The presence of Mo, Se, Co, and P and their homogeneous distributions can be clearly observed in the EDS elemental mapping of $MoSe_2$-Co_2P hybrid nanostructures (Figure S9).

Besides Ni_2P and Co_2P nanoparticles, metallic Ni and Co nanoparticles have also been successfully grown on the surface of $MoSe_2$ nanospheres (see Materials and Methods for details). Figure 3(a) shows that the Ni nanoparticles have been grown on the surface of $MoSe_2$ nanospheres to form the $MoSe_2$-Ni hybrid nanostructures. The size of Ni nanoparticles in the hybrid nanostructures is 7.4 ± 1.5 nm (Figure S10). In the HRTEM image (Figure 3(b)), the measured interplanar distances between lattice fringes are estimated to be 6.89 Å and 2.18 Å, which match well with the (002) planes of $MoSe_2$ and (111) planes of Ni, respectively. The cubic Ni (JCPDS No. 01-1258, $a = 3.54\,Å$) was confirmed by the XRD pattern (Figure S11a). Figure S11b confirms the magnetic property of Ni nanoparticles in the prepared $MoSe_2$-Ni hybrid nanostructures. The EDS (Figure S12) and corresponding elemental mapping (Figure S13) demonstrate the presence of Mo, Se, and Ni and their homogeneous distribution. Using the similar

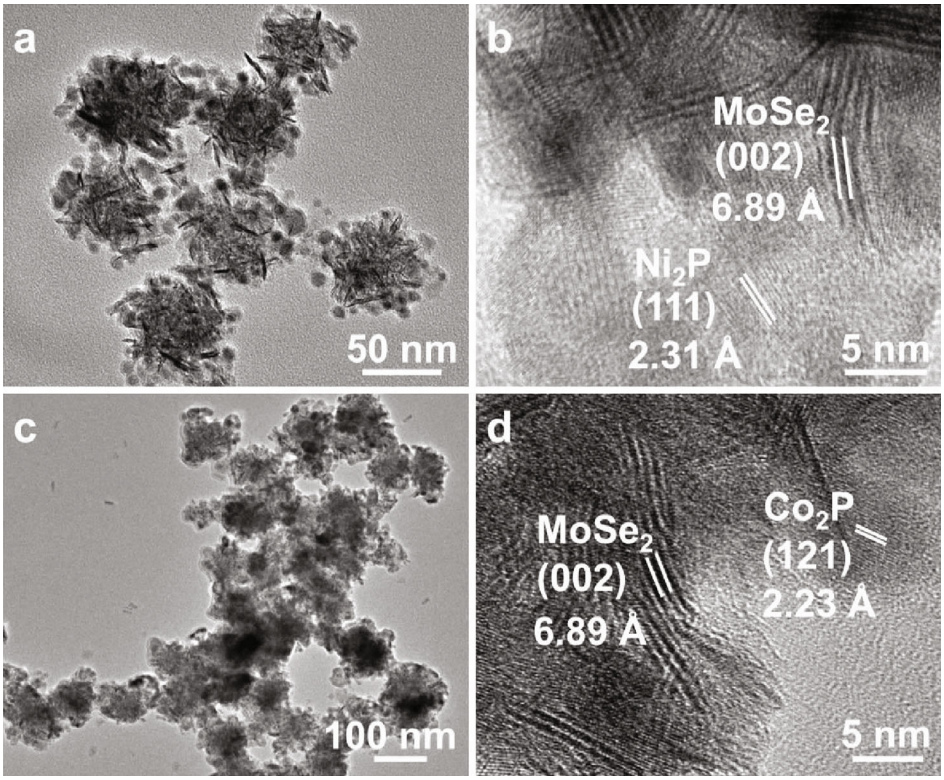


Figure 2: TEM and HRTEM measurements of the $MoSe_2$-Ni_2P and $MoSe_2$-Co_2P hybrid nanostructures. (a) TEM and (b) HRTEM images of $MoSe_2$-Ni_2P hybrid nanostructures. (c) TEM and (d) HRTEM images of $MoSe_2$-Co_2P hybrid nanostructures.

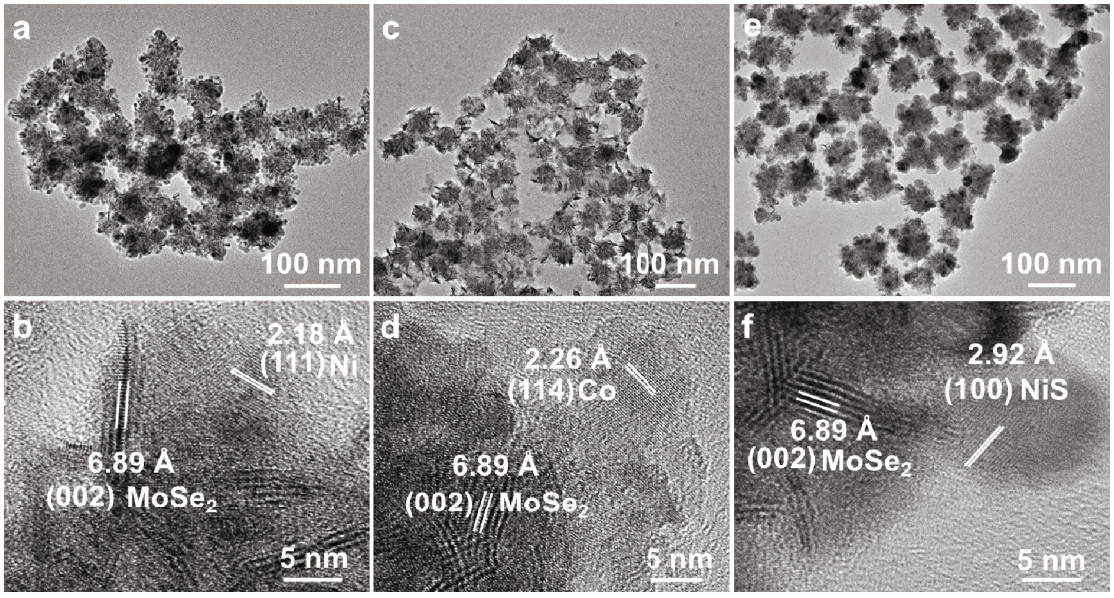


Figure 3: TEM and HRTEM measurements of the $MoSe_2$-Ni, $MoSe_2$-Co, and $MoSe_2$-NiS hybrid nanostructures. (a) TEM and (b) HRTEM images of the $MoSe_2$-Ni hybrid nanostructures. (c) TEM and (d) HRTEM images of the $MoSe_2$-Co hybrid nanostructures. (e) TEM and (f) HRTEM images of the $MoSe_2$-NiS hybrid nanostructures.

method, the $MoSe_2$-Co hybrid nanostructure can also be prepared (Figure 3(c)). The corresponding HRTEM image reveals that the observed lattice spacing for $MoSe_2$ (002) planes and Co (114) planes are 6.89 Å and 2.26 Å, respectively. The size of Co nanoparticles in the hybrid nanostructures is 6.4 ± 1.4 nm (Figure S14). The XRD pattern identifies that the $MoSe_2$ (JCPDS No. 15-0029) and hexagonal phase Co (JCPDS No. 65-9722, $a = 8.288\,Å$, $c = 10.542\,Å$) coexist (Figure S15a). Figure S15b confirms the magnetic property of Co nanoparticles in the prepared $MoSe_2$-Co hybrid nanostructures. Furthermore, the presence of Mo, Se, and Co and their homogeneous distributions

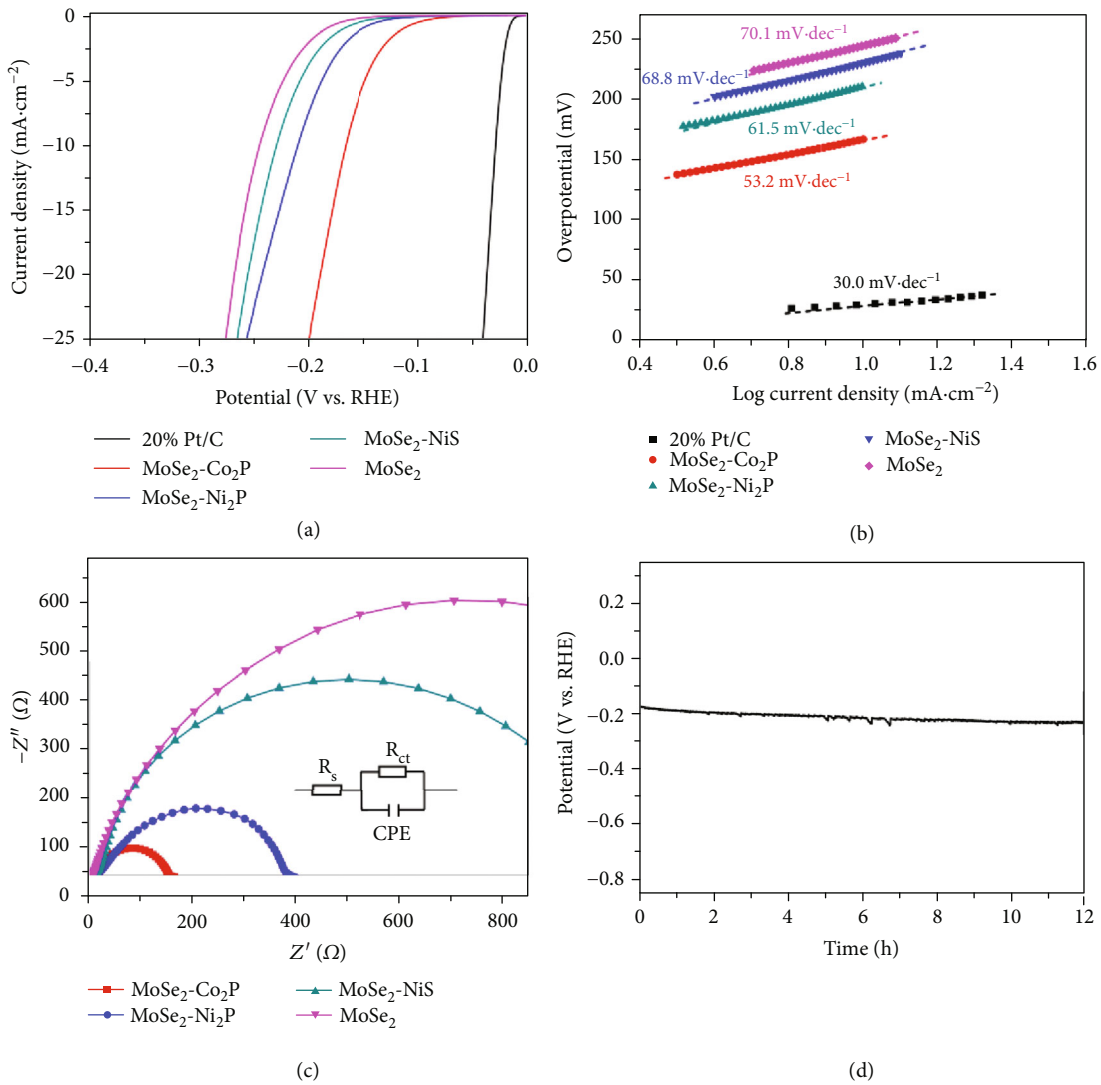


FIGURE 4: HER electrochemical performances of the hybrid nanostructures. (a) Polarization curves of the 20 wt% Pt/C, $MoSe_2$-Co_2P, $MoSe_2$-Ni_2P, and $MoSe_2$-NiS hybrid nanostructures, and $MoSe_2$ nanosphere with iR correction. (b) The corresponding Tafel plots. (c) Nyquist plots of $MoSe_2$-Co_2P, $MoSe_2$-Ni_2P, and $MoSe_2$-NiS hybrid nanostructures and $MoSe_2$ nanosphere collected at a bias voltage of -150 mV. Inset: the equivalent circuit used for fitting the Nyquist plots. (d) Chronopotentiometry response for $MoSe_2$-Co_2P hybrid nanostructures at 10 mA cm^{-2} for 12 h.

have been shown in the EDS spectrum (Figure S16) and corresponding elemental mapping (Figure S17).

Moreover, after the sulfurization of the $MoSe_2$-Ni hybrid nanostructure, the $MoSe_2$-NiS hybrid nanostructure can also be synthesized by adding sulfur precursor to the reaction solution (see Materials and Methods for details). The as-synthesized nanostructure was characterized by XRD (Figure S18). The XRD analysis of the final product reveals a mixture of hexagonal $MoSe_2$ (JCPDS No. 15-0029) and hexagonal NiS (JCPDS No. 02-1273, $a = 3.440$ Å, $c = 5.350$ Å). The TEM image (Figure 3(e)) shows that the NiS nanoparticles are uniformly coated on the surface of the $MoSe_2$ nanospheres. The size of NiS nanoparticles in the hybrid nanostructures is 11.7 ± 1.4 nm (Figure S19). As shown in the corresponding HRTEM image, the lattice spacing of 6.89 Å corresponds to the (002) planes of $MoSe_2$, while the other one of 2.92 Å is attributed to the (100) planes of NiS (Figure 3(f)). The EDS spectrum in Figure S20 shows that the Mo/Se and Ni/S molar ratios are estimated to 1/2.4 and 1/1, respectively, close to the corresponding stoichiometric ratios. The EDS elemental mapping (Figure S21) further demonstrates the homogeneous distributions of Mo, Se, Ni, and S in the as-prepared nanostructure.

As a proof-of-concept application, the aforementioned synthesized hybrid nanostructures, including $MoSe_2$-Ni_2P, $MoSe_2$-Co_2P, and $MoSe_2$-NiS, were used as catalysts for the electrochemical HER. The electrochemical HER activities were tested in 0.5 M H_2SO_4 aqueous solution using a standard three-electrode system. Figure 4(a) shows typical polarization curves of these as-prepared hybrid nanostructures and the 20 wt% Pt/C. The $MoSe_2$ nanosphere shows the lowest HER activity with overpotential of 245 mV at 10 mA cm^{-2}. After growth of NiS, Ni_2P, and Co_2P on the

$MoSe_2$ nanospheres, the catalytic activities of hybrid nanostructures were significantly enhanced. The overpotentials at 10 mA cm^{-2} are 231, 211, and 167 mV for the $MoSe_2$-NiS, $MoSe_2$-Ni_2P, and $MoSe_2$-Co_2P hybrid nanostructures, respectively. Furthermore, the Tafel slopes were used to evaluate the HER kinetics. As shown in Figure 4(b), the measured Tafel slope of Pt/C is 30.0 mV dec^{-1}, close to the reported value [10–12]. The Tafel slope of $MoSe_2$ nanospheres is 70.1 mV/dec, which decreases to 68.8, 61.5, and 53.2 mV/dec for $MoSe_2$-NiS, $MoSe_2$-Ni_2P, and $MoSe_2$-Co_2P hybrid nanostructures, respectively. In addition, as shown in Figure 4(c), the electrochemical impedance spectroscopy (EIS) reveals that these hybrid nanostructures exhibit a faster electron/charge transfer rate than does the $MoSe_2$ nanosphere (Table S1), suggesting that the growth of NiS, Ni_2P, and Co_2P on $MoSe_2$ nanospheres can significantly enhance the electrical conductivity. The good electron-transfer kinetics is important for electrocatalysts to exhibit high activity [55–57]. Note that the performance of $MoSe_2$-Co_2P is comparable to or even better than those previously reported similar materials for the acid HER (Table S2).

It is important to understand the mechanism for the improved HER performance of $MoSe_2$-Co_2P hybrid nanostructures. First, the more postgrowth nanostructures mean the more exposure of active sites, enabling a high utilization ratio of catalysts [58–61]. The effect of the surface area on HER was evaluated through the electrochemical double-layer capacitance (C_{dl}, Figure S22). The fitted C_{dl} of $MoSe_2$-Co_2P is close to that of $MoSe_2$, revealing that the promoted HER performance should be derived from the enhanced intrinsic activity rather than the increased electrochemical active specific area or active sites. On the other hand, the R_{ct} value of the $MoSe_2$-Co_2P hybrid nanostructures is smaller than the pure $MoSe_2$ nanospheres (Table S1), indicating the fastest charge transfer process. These results clearly show the crucial role of the synergetic effect between $MoSe_2$ and Co_2P in $MoSe_2$-Co_2P hybrid nanostructures, which is responsible for the enhanced electrochemical hydrogen evolution.

The stability of the $MoSe_2$-Co_2P hybrid nanostructures for HER catalysis was tested using the chronopotentiometry method. As shown in Figure 4(d), only a slight voltage drop is observed even after 12 h electrolysis of water at current density of 10 mA cm^{-2}, indicating the excellent stability of the $MoSe_2$-Co_2P hybrid nanostructures. Moreover, after the stability test, the polarization curve only shows a slight negative shift (Figure S23) as compared with the initial one. These results imply the long-term stability of $MoSe_2$-Co_2P catalyst for HER.

3. Discussion

In summary, by using the synthesized $MoSe_2$ nanospheres as templates, nickel and cobalt-based nanomaterials can be synthesized on them to form a series of the $MoSe_2$ nanosphere-based hybrid nanostructures, including $MoSe_2$-Ni_2P, $MoSe_2$-Co_2P, $MoSe_2$-Ni, $MoSe_2$-Co, and $MoSe_2$-NiS. Importantly, as a proof-of-concept application, when used as electrocatalysts, the $MoSe_2$-Ni_2P, $MoSe_2$-Co_2P, and $MoSe_2$-NiS hybrid nanostructures exhibited high HER activities in acidic environment. Among them, the $MoSe_2$-Co_2P hybrid nanostructures exhibit excellent stability and highest HER activity with an overpotential of 167 mV at 10 mA cm^{-2}. We believe that as a general method for hybridizing layered TMD nanostructures with transition metal chalcogenide/phosphide nanocrystals, this strategy is applicable for growth of many other nanomaterials to form hybrid nanostructures with enhanced electrochemical activity and stability.

4. Materials and Methods

4.1. Chemicals. Molybdenum chloride ($MoCl_5$) was purchased from Alfa Aesar. Sulfur, selenium, nickel acetylacetonate ($Ni(acac)_2$), cobalt acetylacetonate ($Co(acac)_2$), trioctylphosphine (TOP), octadecene (ODE), stearic acid (SA), oleylamine (OLA), and toluene were purchased from Aldrich. All the chemicals were used as received without further purification.

4.2. Synthesis of $MoSe_2$ Nanosheet-Assembled Nanospheres. In a typical procedure, 0.5 mmol of $MoCl_5$, 1 g of SA, and 9 mL of ODE were added into a 100 mL three-necked flask. The aforementioned mixture, denoted as solution A, was degassed under a vacuum at 120°C for 10 min. Then, the temperature was heated up to 300°C under nitrogen. At the same time, 1 mmol of selenium powder was dissolved into 2 mL of ODE at 250°C, which was denoted as solution B. Solution B was cooled to 130°C and subsequently injected into solution A when the temperature of mixed solution finally reached 300°C, which was then kept at 300°C for 30 min. After it was cooled down to room temperature, the product, i.e., $MoSe_2$ nanospheres, was collected by centrifugation (10000 rpm, 5 min) and washed several times with toluene and acetone (technical grade) before further characterization. All products in this work were collected and washed by the same method.

4.3. Synthesis of $MoSe_2$-Ni_2P, $MoSe_2$-Co_2P, $MoSe_2$-Ni, $MoSe_2$-Co, and $MoSe_2$-NiS Hybrid Nanostructures. In order to synthesize the $MoSe_2$-Ni_2P hybrid nanostructures, the freshly prepared $MoSe_2$ nanospheres were redispersed into 10 mL of OLA containing 0.5 mmol $Ni(acac)_2$ and 2 mL TOP. The mixture was degassed under a vacuum at 110°C for 10 min. Then, the temperature was increased to 320°C under nitrogen atmosphere and kept for 1 h before cooling down to room temperature. The $MoSe_2$-Co_2P hybrid nanostructures were synthesized by the same method, except that $Co(acac)_2$ was used instead of $Ni(acac)_2$. The preparation procedure of $MoSe_2$-Ni and $MoSe_2$-Co hybrid nanostructures was the same as the aforementioned procedure except that the reaction temperature was changed to 220°C from 320°C. For the synthesis of $MoSe_2$-NiS hybrid nanostructures, the procedure was the same as that used for synthesis of $MoSe_2$-Ni hybrid nanostructures, except that after the reaction was proceeded at 220°C for 1 h, 2 mL of sulfur powder (0.5 mmol) in oleylamine (OLA) was injected. The resulting mixed solution was kept at 220°C for another 1 h.

4.4. Characterization. The XRD were recorded on a Bruker D8 diffractometer (German) with a slit of 1/2° at a scanning

rate of 2° min^{-1}, using Cu K_α radiation (λ = 1.5406 Å). TEM, HRTEM, and EDS mapping characterizations were performed on JEOL 2010F (Japan) and JEOL 2100F (Japan) with an acceleration voltage of 200 kV.

4.5. Electrode Preparation. Experimentally, 4 mg of acetylene black was first mixed with 5 mL of hexane and then sonicated to form a uniform suspension. Then, 8 mg of $MoSe_2$, $MoSe_2$-Ni_2P, $MoSe_2$-Co_2P, or $MoSe_2$-NiS in hexane was added into acetylene black suspension under sonication for 1 h. The mixed catalysts were separated by centrifugation, then washed with ethanol. The prepared catalysts were annealed at 400°C for 30 min under a flow 5% H_2/Ar to remove surfactants. 4 mg of the respective catalyst powders was dispersed in 1 mL of 1 : 1 (*v*/*v*) water/ethanol mixed solvents under ultrasonication for 1 h. 5 μL of the resulting solution was dropped onto the surface of a cleaned glassy carbon electrode by a microliter syringe and dried at room temperature. After drying at room temperature, the surface of the catalyst-based electrode was covered by 5 μL of 1% Nafion solution.

4.6. Electrochemical Measurements. All the electrochemical experiments were performed on an electrochemical workstation (CHI 760C, CH Instruments Inc., USA), using a conventional three-electrode system, i.e., a Hg/Hg_2Cl_2 (saturated KCl, SCE) reference electrode, a carbon rod counter electrode, and the prepared working electrode. 0.5 M H_2SO_4 aqueous solution was used as the electrolyte throughout the experiments. Before the electrochemical measurement, the electrolyte was degassed by bubbling N_2 for at least 30 min. The polarization curves were obtained by sweeping the potential from 0 to -0.6 V (vs. SCE) at a sweep rate of 2 mV s^{-1}. Electrochemical impedance spectroscopy (EIS) was recorded in 0.5 M H_2SO_4 aqueous solution using an alternating current (AC) voltage of 5 mV and direct current (DC) voltage of -0.15 V (vs. RHE) within the frequency range from 100 kHz to 0.1 Hz. Voltage-time responses were monitored by chronopotentiometry measurement at 10 mA cm^{-2} for 12 h.

Conflicts of Interest

The authors declare no competing financial interests.

Authors' Contributions

H. Zhang proposed the research direction and guided the project. S. Han synthesized and characterized the materials. K. Zhou measured the electrochemical performance of the materials. S. Han, K. Zhou, Y. Yu, C. Tan, J. Chen, Y. Huang, Q. Ma, Y. Chen, H. Cheng, W. Zhou, and H. Zhang analyzed and discussed the experimental results and drafted the manuscript. Shikui Han and Kai Zhou contributed equally to this work.

Acknowledgments

This work was supported by MOE under AcRF Tier 2 (ARC 19/15; Nos. MOE2014-T2-2-093, MOE2015-T2-2-057, MOE2016-T2-2-103, and MOE2017-T2-1-162) and AcRF Tier 1 (2016-T1-001-147, 2016-T1-002-051, 2017-T1-001-150, and 2017-T1-002-119) and Nanyang Technological University under the Start-Up Grant (M4081296.070.500000) in Singapore. S.H. thanks the support from the Fundamental Research Funds for the Central Universities (No. PA2018GDQT0013) in China. We would like to acknowledge the Facility for Analysis, Characterization, Testing and Simulation, Nanyang Technological University, Singapore, for use of their electron microscopy (and/or X-ray) facilities. H.Z. thanks the support from the Innovation and Technology Commission via the Hong Kong Branch of National Precious Metals Material Engineering Research Center and the Start-Up Grant from the City University of Hong Kong.

Supplementary Materials

Figure S1: XRD pattern of the as-prepared $MoSe_2$ nanosheet-assembled nanospheres. Figure S2: XRD pattern of the as-prepared $MoSe_2$-Ni_2P nanostructures. Figure S3: statistical analysis of the size of 50 Ni_2P nanoparticles measured from HRTEM images. Figure S4: EDS spectrum of the as-prepared $MoSe_2$-Ni_2P nanostructures. Figure S5: EDS mapping of the as-prepared $MoSe_2$-Ni_2P hybrid nanostructures. Figure S6: statistical analysis of the size of 50 Co_2P nanoparticles measured from HRTEM images. Figure S7: XRD pattern of the as-prepared $MoSe_2$-Co_2P hybrid nanostructures. Figure S8: EDS spectrum of the as-prepared $MoSe_2$-Co_2P hybrid nanostructures. Figure S9: EDS elemental mapping of the as-prepared $MoSe_2$-Co_2P hybrid nanostructures. Figure S10: statistical analysis of the size of 50 Ni nanoparticles measured from HRTEM images. Figure S11: (a) XRD pattern of the as-prepared $MoSe_2$-Ni hybrid nanostructures. (b) Top: photograph of $MoSe_2$-Ni in toluene. Bottom: photograph showing the magnetic property of $MoSe_2$-Ni in toluene in the presence of a magnet. Figure S12: EDS spectrum of the as-prepared $MoSe_2$-Ni hybrid nanostructures. Figure S13: EDS elemental mapping of the as-prepared $MoSe_2$-Ni hybrid nanostructures. Figure S14: statistical analysis of the size of 50 Co nanoparticles measured from HRTEM images. Figure S15: (a) XRD pattern of the as-prepared $MoSe_2$-Co hybrid nanostructures. (b) Top: photograph of $MoSe_2$-Co in toluene. Bottom: photograph showing the magnetic property of $MoSe_2$-Co in toluene in the presence of a magnet. Figure S16: EDS spectrum of the as-prepared $MoSe_2$-Co hybrid nanostructures. Figure S17: EDS elemental mapping of the as-prepared $MoSe_2$-Co hybrid nanostructures. Figure S18: XRD pattern of the as-prepared $MoSe_2$-NiS hybrid nanostructures. Figure S19: statistical analysis of the size of 50 NiS nanoparticles measured from HRTEM images. Figure S20: EDS spectrum of the as-prepared $MoSe_2$-NiS hybrid nanostructures. Figure S21: EDS elemental mapping of the as-prepared $MoSe_2$-NiS hybrid nanostructures. Figure S22: cyclic voltammetry curves of (a) $MoSe_2$-Co_2P hybrid nanostructures and (b) $MoSe_2$ nanosphere in the region of 0.15-0.25 V vs. RHE. (c) The differences in current density at 0.20 V vs. RHE plotted against scan rate fits to a linear regression. Figure S23: polarization curves of $MoSe_2$-Co_2P hybrid nanostructures before and after

12 h-HER tests at 10 mA cm^{-2}. Table S1: the charge transfer resistances (R_{ct}) and constant phase elements (CPEs) of the prepared electrocatalysts. Table S2: HER activities of the $MoSe_2$-Co_2P hybrid nanostructures and the reported electrocatalysts. *(Supplementary Materials)*

References

[1] M. Caban-Acevedo, M. L. Stone, J. R. Schmidt et al., "Efficient hydrogen evolution catalysis using ternary pyrite-type cobalt phosphosulphide," *Nature Materials*, vol. 14, no. 12, pp. 1245–1251, 2015.

[2] J. F. Xie, J. J. Zhang, S. Li et al., "Controllable disorder engineering in oxygen-incorporated MoS_2 ultrathin nanosheets for efficient hydrogen evolution," *Journal of the American Chemical Society*, vol. 135, no. 47, pp. 17881–17888, 2013.

[3] G. Glenk and S. Reichelstein, "Economics of converting renewable power to hydrogen," *Nature Energy*, vol. 4, no. 3, pp. 216–222, 2019.

[4] D. C. Upham, V. Agarwal, A. Khechfe et al., "Catalytic molten metals for the direct conversion of methane to hydrogen and separable carbon," *Science*, vol. 358, no. 6365, pp. 917–921, 2017.

[5] J. Greeley, T. F. Jaramillo, J. Bonde, I. B. Chorkendorff, and J. K. Norskov, "Computational high-throughput screening of electrocatalytic materials for hydrogen evolution," *Nature Materials*, vol. 5, no. 11, pp. 909–913, 2006.

[6] M. Chhowalla, H. S. Shin, G. Eda, L. J. Li, K. P. Loh, and H. Zhang, "The chemistry of two-dimensional layered transition metal dichalcogenide nanosheets," *Nature Chemistry*, vol. 5, no. 4, pp. 263–275, 2013.

[7] H. Zhang, "Ultrathin two-dimensional nanomaterials," *ACS Nano*, vol. 9, no. 10, pp. 9451–9469, 2015.

[8] Q. Lu, A.-L. Wang, Y. Gong et al., "Crystal phase - based epitaxial growth of hybrid noble metal nanostructures on 4 h/Fcc Au nanowires," *Nature Chemistry*, vol. 10, no. 4, pp. 456–461, 2018.

[9] X. Zhang, Z. Luo, P. Yu et al., "Lithiation-induced amorphization of $Pd_3P_2S_8$ for highly efficient hydrogen evolution," *Nature Catalysis*, vol. 1, no. 6, pp. 460–468, 2018.

[10] M. R. Gao, J. X. Liang, Y. R. Zheng et al., "An efficient molybdenum disulfide/cobalt diselenide hybrid catalyst for electrochemical hydrogen generation," *Nature Communications*, vol. 6, no. 1, article 5982, 2015.

[11] J. Zhang, T. Wang, D. Pohl et al., "Interface engineering of MoS_2/Ni_3S_2 heterostructures for highly enhanced electrochemical overall-water-splitting activity," *Angewandte Chemie International Edition*, vol. 55, no. 23, pp. 6702–6707, 2016.

[12] X. B. Ge, L. Y. Chen, L. Zhang, Y. R. Wen, A. Hirata, and M. W. Chen, "Nanoporous metal enhanced catalytic activities of amorphous molybdenum sulfide for high-efficiency hydrogen production," *Advanced Materials*, vol. 26, no. 19, pp. 3100–3104, 2014.

[13] C. Tan, X. Cao, X.-J. Wu et al., "Recent advances in ultrathin two-dimensional nanomaterials," *Chemical Reviews*, vol. 117, no. 9, pp. 6225–6331, 2017.

[14] K. Chang, X. Hai, H. Pang et al., "Targeted synthesis of 2H- and 1T-phase MoS_2 monolayers for catalytic hydrogen evolution," *Advanced Materials*, vol. 28, no. 45, pp. 10033–10041, 2016.

[15] D. Voiry, J. Yang, and M. Chhowalla, "Recent strategies for improving the catalytic activity of 2D TMD nanosheets toward the hydrogen evolution reaction," *Advanced Materials*, vol. 28, no. 29, pp. 6197–6206, 2016.

[16] L. Cheng, W. Huang, Q. Gong et al., "Ultrathin WS_2 nanoflakes as a high - performance electrocatalyst for the hydrogen evolution reaction," *Angewandte Chemie International Edition*, vol. 53, no. 30, pp. 7860–7863, 2014.

[17] S. Han, X. Yang, Y. Zhu et al., "Synthesis of WO_n-WX_2 (n=2.7, 2.9; X=S, Se) heterostructures for highly efficient green quantum dot light-emitting diodes," *Angewandte Chemie International Edition*, vol. 56, no. 35, pp. 10486–10490, 2017.

[18] Y. Yu, G.-H. Nam, Q. He et al., "High phase-purity 1T′-MoS_2 and 1T′-$MoSe_2$ layered crystals," *Nature Chemistry*, vol. 10, no. 6, pp. 638–643, 2018.

[19] Z. W. Zhang, P. Chen, X. D. Duan, K. T. Zang, J. Luo, and X. F. Duan, "Robust epitaxial growth of two-dimensional heterostructures, multiheterostructures, and superlattices," *Science*, vol. 357, no. 6353, pp. 788–792, 2017.

[20] J. Chen, X.-J. Wu, Y. Gong et al., "Edge epitaxy of two-dimensional $MoSe_2$ and MoS_2 nanosheets on one-dimensional nanowires," *Journal of the American Chemical Society*, vol. 139, no. 25, pp. 8653–8660, 2017.

[21] H. F. Lin, Y. Y. Li, H. Y. Li, and X. Wang, "Multi-node CdS hetero-nanowires grown with defect-rich oxygen-doped MoS_2 ultrathin nanosheets for efficient visible-light photocatalytic H_2 evolution," *Nano Research*, vol. 10, no. 4, pp. 1377–1392, 2017.

[22] Z. Huang, W. Luo, L. Ma et al., "Dimeric $[Mo_2S_{12}]^{2-}$ cluster: a molecular analogue of MoS_2 edges for superior hydrogen-evolution electrocatalysis," *Angewandte Chemie International Edition*, vol. 54, no. 50, pp. 15181–15185, 2015.

[23] J. Xu, J. Cui, C. Guo et al., "Ultrasmall Cu_7S_4@MoS_2 heteronanoframes with abundant active edge sites for ultrahigh-performance hydrogen evolution," *Angewandte Chemie International Edition*, vol. 55, no. 22, pp. 6502–6505, 2016.

[24] D. Voiry, H. Yamaguchi, J. Li et al., "Enhanced catalytic activity in strained chemically exfoliated WS_2 nanosheets for hydrogen evolution," *Nature Materials*, vol. 12, no. 9, pp. 850–855, 2013.

[25] W. Liu, E. Hu, H. Jiang et al., "A highly active and stable hydrogen evolution catalyst based on pyrite-structured cobalt phosphosulfide," *Nature Communications*, vol. 7, article 10771, 2016.

[26] E. J. Popczun, J. R. McKone, C. G. Read et al., "Nanostructured nickel phosphide as an electrocatalyst for the hydrogen evolution reaction," *Journal of the American Chemical Society*, vol. 135, no. 25, pp. 9267–9270, 2013.

[27] Q. Liu, J. Q. Tian, W. Cui et al., "Carbon nanotubes decorated with CoP nanocrystals: a highly active non-noble-metal nanohybrid electrocatalyst for hydrogen evolution," *Angewandte Chemie International Edition*, vol. 53, no. 26, pp. 6710–6714, 2014.

[28] X. G. Wang, Y. V. Kolen'ko, X. Q. Bao, K. Kovnir, and L. F. Liu, "One-step synthesis of self-supported nickel phosphide nanosheet array cathodes for efficient electrocatalytic hydrogen generation," *Angewandte Chemie International Edition*, vol. 54, no. 28, pp. 8188–8192, 2015.

[29] J. Kibsgaard, Z. B. Chen, B. N. Reinecke, and T. F. Jaramillo, "Engineering the surface structure of MoS_2 to preferentially expose active edge sites for electrocatalysis," *Nature Materials*, vol. 11, no. 11, pp. 963–969, 2012.

[30] H. Li, C. Tsai, A. L. Koh et al., "Activating and optimizing MoS_2 basal planes for hydrogen evolution through the formation of strained sulphur vacancies," *Nature Materials*, vol. 15, no. 1, pp. 48–53, 2016.

[31] Y. G. Li, H. L. Wang, L. M. Xie, Y. Y. Liang, G. S. Hong, and H. J. Dai, "MoS_2 nanoparticles grown on graphene: an advanced catalyst for the hydrogen evolution reaction," *Journal of the American Chemical Society*, vol. 133, no. 19, pp. 7296–7299, 2011.

[32] J. D. Benck, T. R. Hellstern, J. Kibsgaard, P. Chakthranont, and T. F. Jaramillo, "Catalyzing the hydrogen evolution reaction (HER) with molybdenum sulfide nanomaterials," *ACS Catalysis*, vol. 4, no. 11, pp. 3957–3971, 2014.

[33] Y. Yan, B. Y. Xia, Z. C. Xu, and X. Wang, "Recent development of molybdenum sulfides as advanced electrocatalysts for hydrogen evolution reaction," *ACS Catalysis*, vol. 4, no. 6, pp. 1693–1705, 2014.

[34] H. T. Wang, Z. Y. Lu, D. S. Kong, J. Sun, T. M. Hymel, and Y. Cui, "Electrochemical tuning of MoS_2 nanoparticles on three-dimensional substrate for efficient hydrogen evolution," *ACS Nano*, vol. 8, no. 5, pp. 4940–4947, 2014.

[35] C. Tsai, K. R. Chan, F. Abild-Pedersen, and J. K. Nørskov, "Active edge sites in $MoSe_2$ and WSe_2 catalysts for the hydrogen evolution reaction: a density functional study," *Physical Chemistry Chemical Physics*, vol. 16, no. 26, pp. 13156–13164, 2014.

[36] X. L. Zhou, Y. Liu, H. X. Ju et al., "Design and epitaxial growth of $MoSe_2$-NiSe vertical heteronanostructures with electronic modulation for enhanced hydrogen evolution reaction," *Chemistry of Materials*, vol. 28, no. 6, pp. 1838–1846, 2016.

[37] X. L. Zhou, J. Jiang, T. Ding et al., "Fast colloidal synthesis of scalable Mo-rich hierarchical ultrathin $MoSe_{2-x}$ nanosheets for high-performance hydrogen evolution," *Nanoscale*, vol. 6, no. 19, pp. 11046–11051, 2014.

[38] F. H. Saadi, A. I. Carim, J. M. Velazquez et al., "*Operando* synthesis of macroporous molybdenum diselenide films for electrocatalysis of the hydrogen-evolution reaction," *ACS Catalysis*, vol. 4, no. 9, pp. 2866–2873, 2014.

[39] Y. Yang, S. T. Wang, J. C. Zhang, H. Y. Li, Z. L. Tang, and X. Wang, "Nanosheet-assembled $MoSe_2$ and S-doped $MoSe_{2-x}$ nanostructures for superior lithium storage properties and hydrogen evolution reactions," *Inorganic Chemistry Frontiers*, vol. 2, no. 10, pp. 931–937, 2015.

[40] Z. Gholamvand, D. McAteer, C. Backes et al., "Comparison of liquid exfoliated transition metal dichalcogenides reveals $MoSe_2$ to be the most effective hydrogen evolution catalyst," *Nanoscale*, vol. 8, no. 10, pp. 5737–5749, 2016.

[41] Z. Y. Lei, S. J. Xu, and P. Y. Wu, "Ultra-thin and porous $MoSe_2$ nanosheets: facile preparation and enhanced electrocatalytic activity towards the hydrogen evolution reaction," *Physical Chemistry Chemical Physics*, vol. 18, no. 1, pp. 70–74, 2016.

[42] J. Kibsgaard and T. F. Jaramillo, "Molybdenum phosphosulfide: an active, acid-stable, earth-abundant catalyst for the hydrogen evolution reaction," *Angewandte Chemie International Edition*, vol. 53, no. 52, pp. 14433–14437, 2014.

[43] P. Jiang, Q. Liu, Y. H. Liang, J. Q. Tian, A. M. Asiri, and X. P. Sun, "A cost-effective 3d hydrogen evolution cathode with high catalytic activity: FeP nanowire array as the active phase," *Angewandte Chemie-International Edition*, vol. 53, no. 47, pp. 12855–12859, 2014.

[44] J. M. McEnaney, J. C. Crompton, J. F. Callejas et al., "Amorphous molybdenum phosphide nanoparticles for electrocatalytic hydrogen evolution," *Chemistry of Materials*, vol. 26, no. 16, pp. 4826–4831, 2014.

[45] J. M. McEnaney, J. C. Crompton, J. F. Callejas et al., "Electrocatalytic hydrogen evolution using amorphous tungsten phosphide nanoparticles," *Chemical Communications*, vol. 50, no. 75, pp. 11026–11028, 2014.

[46] P. Xiao, W. Chen, and X. Wang, "A review of phosphide-based materials for electrocatalytic hydrogen evolution," *Advanced Energy Materials*, vol. 5, no. 24, article 1500985, 2015.

[47] R. Ye, P. del Angel-Vicente, Y. Liu et al., "High-performance hydrogen evolution from $MoS_{2(1-x)}P_x$ solid solution," *Advanced Materials*, vol. 28, no. 7, pp. 1427–1432, 2016.

[48] D. E. Schipper, Z. Zhao, H. Thirumalai et al., "Effects of catalyst phase on the hydrogen evolution reaction of water splitting: preparation of phase-pure films of FeP, Fe_2P, and Fe_3P and their relative catalytic activities," *Chemistry of Materials*, vol. 30, no. 10, pp. 3588–3598, 2018.

[49] Z. S. Wu, L. Huang, H. Liu, and H. L. Wang, "Element-specific restructuring of anion- and cation-substituted cobalt phosphide nanoparticles under electrochemical water-splitting conditions," *ACS Catalysis*, vol. 9, no. 4, pp. 2956–2961, 2019.

[50] F. Yu, H. Q. Zhou, Y. F. Huang et al., "High-performance bifunctional porous non-noble metal phosphide catalyst for overall water splitting," *Nature Communications*, vol. 9, no. 1, article 2551, 2018.

[51] J. Q. Tian, Q. Liu, A. M. Asiri, and X. P. Sun, "Self-supported nanoporous cobalt phosphide nanowire arrays: an efficient 3D hydrogen-evolving cathode over the wide range of pH 0-14," *Journal of the American Chemical Society*, vol. 136, no. 21, pp. 7587–7590, 2014.

[52] A. B. Laursen, K. R. Patraju, M. J. Whitaker et al., "Nanocrystalline Ni_5P_4: a hydrogen evolution electrocatalyst of exceptional efficiency in both alkaline and acidic media," *Energy & Environmental Science*, vol. 8, no. 3, pp. 1027–1034, 2015.

[53] J. F. Callejas, C. G. Read, E. J. Popczun, J. M. McEnaney, and R. E. Schaak, "Nanostructured Co_2P electrocatalyst for the hydrogen evolution reaction and direct comparison with morphologically equivalent CoP," *Chemistry of Materials*, vol. 27, no. 10, pp. 3769–3774, 2015.

[54] C. D. Wang, J. Jiang, T. Ding, G. H. Chen, W. J. Xu, and Q. Yang, "Monodisperse ternary NiCoP nanostructures as a bifunctional electrocatalyst for both hydrogen and oxygen evolution reactions with excellent performance," *Advanced Materials Interfaces*, vol. 3, no. 4, article 1500454, 2016.

[55] J. Wang, K. Li, H. Zhong et al., "Synergistic effect between metal–nitrogen–carbon sheets and NiO nanoparticles for enhanced electrochemical water-oxidation performance," *Angewandte Chemie International Edition*, vol. 54, no. 36, pp. 10530–10534, 2015.

[56] J. Wang, H. Zhong, Z. Wang, F. Meng, and X. Zhang, "Integrated three-dimensional carbon paper/carbon tubes/cobalt-sulfide sheets as an efficient electrode for overall water splitting," *ACS Nano*, vol. 10, no. 2, pp. 2342–2348, 2016.

[57] H. Zhong, J. Wang, F. Meng, and X. Zhang, "In situ activating ubiquitous rust towards low-cost, efficient, free-standing, and recoverable oxygen evolution electrodes," *Angewandte Chemie International Edition*, vol. 55, no. 34, pp. 9937–9941, 2016.

[58] F. Meng, Z. Wang, H. Zhong, J. Wang, J. Yan, and X. Zhang, "Reactive multifunctional template-induced preparation of Fe-N-doped mesoporous carbon microspheres towards highly efficient electrocatalysts for oxygen reduction," *Advanced Materials*, vol. 28, no. 36, pp. 7948–7955, 2016.

[59] Z. Wang, X. Hao, Z. Jiang et al., "C and N hybrid coordination derived Co–C–N complex as a highly efficient electrocatalyst for hydrogen evolution reaction," *Journal of the American Chemical Society*, vol. 137, no. 48, pp. 15070–15073, 2015.

[60] Z. Wang, D. Xu, H. Zhong, J. Wang, F. Meng, and X. Zhang, "Gelatin-derived sustainable carbon-based functional materials for energy conversion and storage with controllability of structure and component," *Science Advances*, vol. 1, no. 1, article e1400035, 2015.

[61] H. Zhong, K. Li, Q. Zhang et al., "In situ anchoring of Co_9S_8 nanoparticles on N and S Co-doped porous carbon tube as bifunctional oxygen electrocatalysts," *NPG Asia Materials*, vol. 8, no. 9, article e308, 2016.